Carbon 102 (2016) 513–519

Contents lists available at ScienceDirect

Carbon

journal homepage: www.elsevier.com/locate/carbon

The effect of a convection vortex on sock formation in the floating catalyst method for carbon nanotube synthesis

Guangfeng Hou [a, *], Ruitao Su [b], Anli Wang [a], Vianessa Ng [a], Weifeng Li [a], Yi Song [a], Lu Zhang [a], Murali Sundaram [a], Vesselin Shanov [a], David Mast [c], David Lashmore [d], Mark Schulz [a, **], Yijun Liu [a]

[a] Department of Mechanical and Materials Engineering, University of Cincinnati, OH 45221, United States
[b] Department of Mechanical Engineering, University of Minnesota, MN 55455, United States
[c] Department of Physics, University of Cincinnati, OH 45221, United States
[d] Department of Materials Science, University of New Hampshire, NH 03824, United States

ARTICLE INFO

Article history:
Received 16 November 2015
Received in revised form
9 February 2016
Accepted 27 February 2016
Available online 2 March 2016

ABSTRACT

The formation of an aerogel-like sock is important to the floating catalyst method of synthesizing carbon nanotubes (CNTs). The sock, a term coined by Alan Windle, is an assembly of the individual electrostatically assembled nanotubes synthesized in the reactor. The coherency of this sock helps form the yarn or sheet. In this study, sock formation is investigated by controlling the feedstock type, injection rate, and carrier gas flow rate. A convection vortex has been identified, possibly for the first time, in the floating catalyst method. A convection vortex model is proposed to explain the sock formation. The sock morphology is found to be strongly affected by the carrier gas flowrate, where too high gas flowrate reduces the concentration of CNTs in the reactor resulting a failure in the sock formation. The dynamic behavior of the sock is explained by a web-shell structure.

1. Introduction

The floating catalyst method [1–3] is one of the most promising methods for scale-up of CNT production. The process includes catalyst formation, chemical decomposition of feedstock under high temperature, and CNT growth, culminating in sock formation. Under precise conditions, the CNT grown in the reactor self-assembles into an aerogel-like sock, which can be densified by stretching and condensation to produce CNT yarn and film [4–8]. The sock is the critical link bridging the nano-scale CNT with macro-scale products because it allows macromanipulation of a nano entity. To optimize the properties of CNT yarn and film, a full understanding of the process, including knowledge of catalyst dynamics, CNT growth, sock formation and post-treatment is needed.

Previous studies of the catalyst dynamics and CNT growth have shown that, it is vital to regulate the sulfur concentration [3,9–12], feedstock injection temperature [10,13], carrier gas flow rate [14,15] and type of hydrocarbon [2,16] in order to control the CNT diameter and purity. There are also intensive studies performed on yarn and film properties in recent years [17–21].

Some simulation studies provided insightful knowledge, regarding catalyst particle activity [22–24], hydrocarbon decomposition [25], and CNT growth [26]. Kuwana et al. [27] observed vortex formation for substrate-based growth of CNTs from simulation study. They suggested that the vortex could be used to enhance the reaction.

Several studies have shed light on the sock formation process. Motta et al. [16] studied the effect of carrier gas and feedstock injection rate on the sock “spinnability” in a vertical furnace. Some mechanisms have been proposed for the sock formation, including thermophoresis or inertial migration [22], van der Waals attraction [7,28] and electrostatic attraction [29]. However, there is still significant ambiguity surrounding the understanding of how transport issues affecting the sock formation process. Furthermore, to the best of our knowledge, there have not been any studies of the sock formation for the horizontal furnace and in particular those parameters affecting sock behavior in the horizontal furnace.

In this work, we present a systematical study of the conditions

* Corresponding author.
** Corresponding author.
E-mail addresses: hougg@mail.uc.edu (G. Hou), Mark.J.Schulz@uc.edu (M. Schulz).

http://dx.doi.org/10.1016/j.carbon.2016.02.087
0008-6223/

for sock formation in a horizontal floating catalyst reactor. On the basis of experimental observations and numerical simulation, we propose a convection vortex model to describe the sock formation process. A web-shell structure has been used to study the sock dynamics.

2. Experimental

2.1. Horizontal floating catalyst reactor

A horizontal reactor is employed for the experiments (Fig. 1). The set-up is equipped with an nubulizer, a high temperature heating furnace, a ceramic reactor tube of 1 m in length with an inner diameter of 45 mm, and a harvest box. If not explicitly stated elsewhere, the feedstock is a mixture of hexane (10 vol%, Fisher Scientific), methanol (90 vol%, Fisher Scientific), ferrocene (1 wt%, Sigma Aldrich) and thiophene (0.3 vol%, Sigma Aldrich). Several carbon sources have been tested on our horizontal furnace, including hexane/methanol, ethanol and butanol. Among them, hexane/methanol provides the most stable sock production. Thus they are used in our experiments. For preparation of the feedstock, hexane and methanol are mixed first, follwed by dissolving ferrocene and thiophene in the mixer. The heating zone temperature is 1400 °C. In the experiments, the Fe/S atomic ratio is kept constant when varying the ferrocene concentration by adjusting the amount of thiophene in the feedstock. Argon gas with 3 vol% hydrogen (100–4000 sccm, Wright Brothers, Inc) and the feedstock are injected together into the tube via a nebulizer. There are three stages in the process: (i) feedstock evaporation and decomposition, (ii) CNT growth, and (iii) sock formation. The feedstock mixture evaporates once entering the high temperature zone after injection. The high temperature induces feedstock decomposition into iron catalyst particles and a carbon source. CNTs then grow from the catalyst particles and aggregate into a sock near the outlet of the reactor tube. A video or digital camera was placed facing the outlet end of the tube, so that the sock dynamics in the reactor tube could be observed and analyzed.

2.2. Characterizations

In all the experiments, the sock exits the reactor tube by itself without intervention. The sock samples were characterized using Raman spectroscopy (Renishaw, inVia, excited by a 514 nm He–Ne laser with spot size of ~1 μm^2), a FEI CM20 transmission electron microscope (TEM), and by thermogravimetric analysis (TGA), using a Netzsch STA409 analyzer (samples were heated up from room temperature to 900 °C at a rate of 10 °C min^{-1} in 30 ml min^{-1} of air).

3. Results and discussion

3.1. Modeling and simulation

Similar as other researchers [22,27], a three-dimensional, steady and compressible flow model has been used for the computational fluid dynamics (CFD) simulation. Using governing equaitons [30,31] for fluid dynamics and heat transfer listed below, the flow field and temperature field in the reactor were computed using ANSYS software [32], ignoring the influence of CNTs in the reactor.

$$\nabla\cdot(\rho\mathbf{u}) = 0 \tag{1}$$

$$\rho\mathbf{u}\cdot\nabla\mathbf{u} = -\nabla p + \nabla\cdot\left(\mu\left(\nabla\mathbf{u} + (\nabla\mathbf{u})^T\right) - \frac{2}{3}\mu(\nabla\cdot\mathbf{u})\mathbf{I}\right) + \rho\mathbf{g} \tag{2}$$

$$\rho C_p\mathbf{u}\cdot\nabla T = \nabla\cdot(k\nabla T) + Q. \tag{3}$$

Here ρ is the gas density, which changes with temperature, $\mathbf{u}$ is the gas velocity field, p is pressure, μ is dynamic viscosity, C_p is the specific heat capacity at constant pressure, T is temperature, k is thermal conductivity and Q is heat generated from chemical reaction.

Using (i) the tube heating zone temperature, (ii) the defined inlet flowrate and (iii) atmospheric pressure, we calculate the gas flow streamline and gas temperature distribution from equations (1)–(3). The simulation results are shown in Fig. 2.

3.2. Sock formation by the convection vortex

There are several studies of the sock formation mechanism for example, (i) it was believed that the sock forms possibly due to thermophoresis or inertial migration, and the CNT may accumulate at a certain distance away from the wall [22]. The thermophoretic force is a result of temperature gradients and responsible for keeping CNTs from bonding on the reactor tube. Also (ii) Zhong et al. [7,28] speculated that the van der Waals attraction leads to the

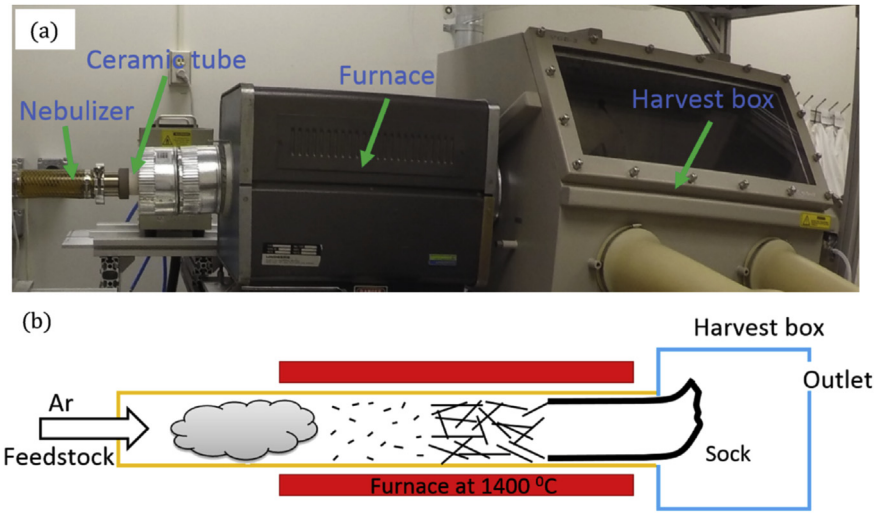

Fig. 1. The horizontal reactor: (a) experimental setup in the labrotary; (b) schematic of the setup. (A color version of this figure can be viewed online.)

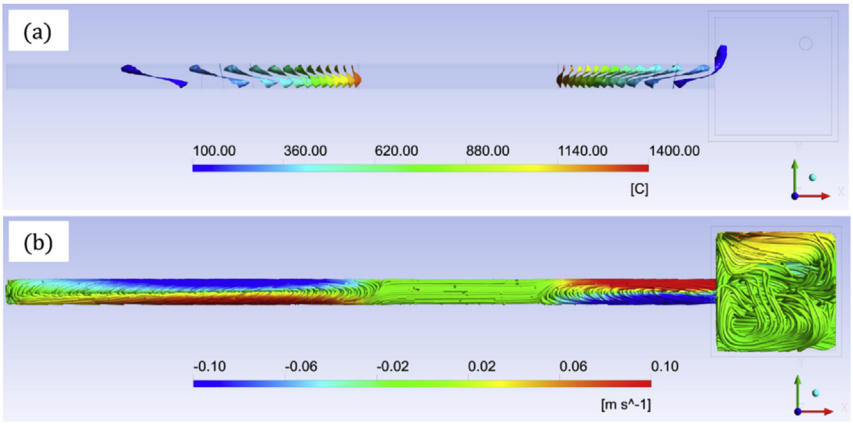

Fig. 2. Simulation of the temperature and flow profiles in the reactor tube: (a) Temperature isosurface, color indicates temperature; (b) velocity streamline. Color indicates gas velocity along the tube axis, the red line shows flow toward the harvest box (right of figure) or outlet of the reactor, the blue line shows flow in the reverse direction toward the inlet of the reactor. The heating zone temperature is 1400 °C, and the gas flowrate is 1000 sccm. (A color version of this figure can be viewed online.)

sock formation. And (iii) Chaffee et al. [29] mentioned that the nanotubes could form bundles due to electrostatic attraction.

In this study, we propose a more complete mechanism, that convection vortex coupled with electrostatic interactions, enables sock formation. Around the outlet region of the reactor tube, there is gas flowing from the harvest box back into the tube (Fig. 3, blue arrows), which interact with the carrier gas flowing out of the tube into the harvest box (red arrows). In the region where the two flows interact (Fig. 3b), CNT flows upwards. Later around the tube outlet, strong velocity flow (around 0.5 m/s) is generated, which is quite high compared with the average flow speed of 0.01 m/s in the middle of the tube. It is noted that the CNTs flow path is intertwined (Fig. 3a) instead of laminar flow, which is responsible for the vortex generated (Fig. 4). This localized high velocity flow and complex flow pattern could lead to connected CNT networks, formed by CNTs coming into close proximity. Similar as flow-induced alignment in wet spinning processing [8], the high velocity and ensuing high drag force cause the CNT to align and self-connect, which creates the closed end of the sock. With more CNTs joining the sock end by the carrier gas flow, this closed end servers as a seed for further sock shell formation. Once the sock is complete, carrier gas flow will push the sock out, forming a continuous CNT sock.

Using a digital camera, a vortex (Fig. 4) around the tube outlet region was observed, which agrees well with the simulation. When there is a low concentration of catalyst particles in the reactor, CNT nucleation is reduced and amorphous carbon tend to form. In this situation, the flow pattern of the CNT and black smoke (possibly amorphous carbon) follows the same path as predicted in the simulation (Fig. 4a and b). When the sock forms, it interacts with the flow field, the sock formation pattern still resembles the simulated flow pattern, although not perfectly. The resemblance between the simulation and sock images shows that the convection vortex plays a key role in the sock behavior.

It is observed that when the sock forms, a closed-end cap forms first, which flows upward and move towards the tube outlet, then the CNT sock continuously comes out of the reactor. Fig. 5 is an example of the entire sock formation process which is also captured on video (see supplementary material). In the process, the CNTs connect with each other forming a closed end around the vortex region. Later, this closed end flows out of the reactor tube, followed by a continuous sock flows, with pattern affected by the vortex flow.

Supplementary video related to this article can be found at http://dx.doi.org/10.1016/j.carbon.2016.02.087

It is important to note that there is also a convection vortex at the inlet region of the reactor tube (Fig. 2). This vortex is believed to have a tremendous effect on the catalyst size, due to the particular flow velocity profile [13]. The increase of the mean free path and residence time of the catalyst particle could affect the concentration of appropriate sized catalyst. This is being further investigated and will be presented in a future publication.

The properties of the produced CNT sock has been characterized (Fig. 6). The high G/D ratio of 25 and TGA analysis showed the good

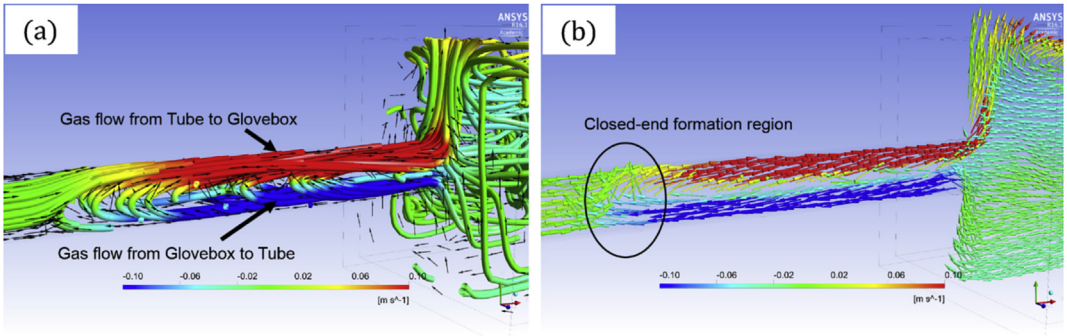

Fig. 3. Convection vortex induced sock formation: (a) Gas streamline in the outlet region; (b) Cross-section arrow volume line showing the region where the sock closed end forms. Color indicates the gas velocity along the tube axis, the red line shows flow toward the harvest box, the blue line shows flow in reverse. In the simulation, the heating zone temperature is 1400 °C for our system, with gas flow rate 1000 sccm. (A color version of this figure can be viewed online.)

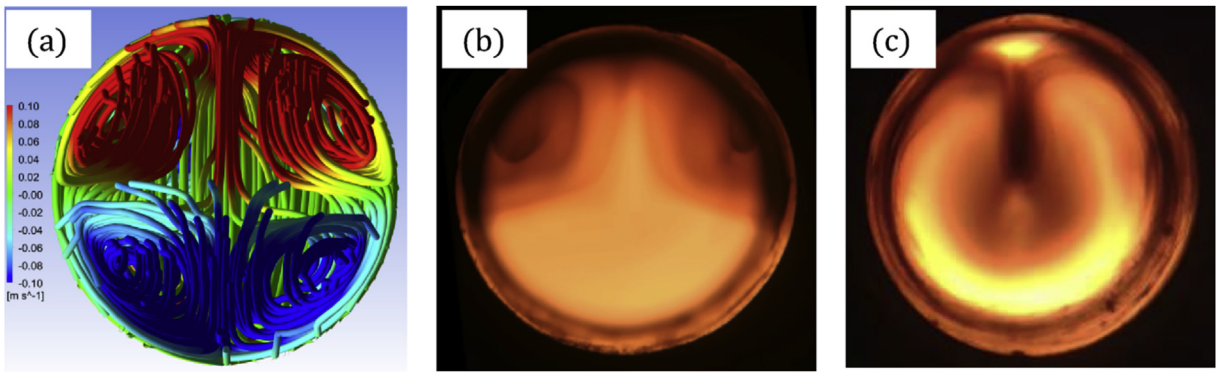

Fig. 4. Outlet vortex comparison from simulation and experiment: (a) Modeled convection vortex around the reactor outlet. The red line indicates the CNT flow path and the blue line indicates gas flow from the harvest box into the reactor. The flowrate is 1000 sccm in simulation; (b) Image showing accumulation of CNTs *without* sock formation, ferrocene concentration is 0.3 wt%, gas flowrate is 1000 sccm, and feedstock injection rate is 16 ml/h; (c) Image showing the sock in the reactor, ferrocene concentration is 1 wt%, gas flowrate is 1800 sccm, feedstock injection rate is 32 ml/h. (A color version of this figure can be viewed online.)

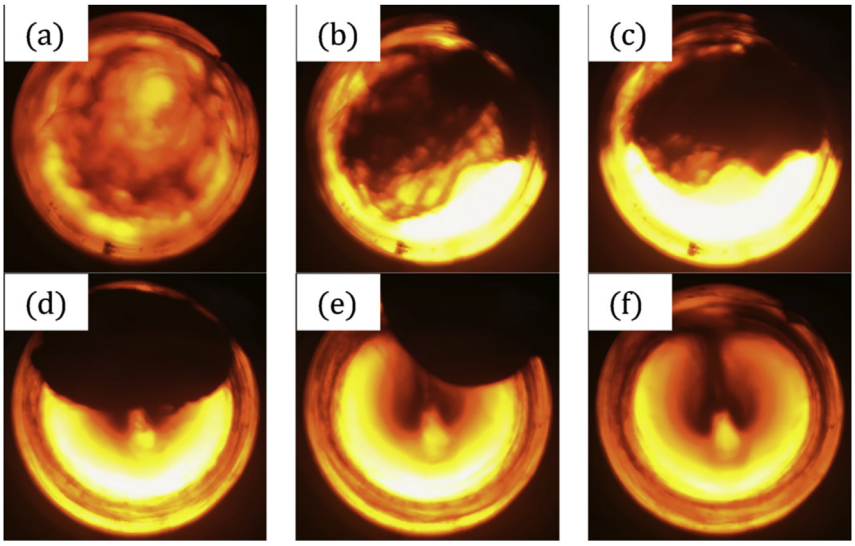

Fig. 5. Sequential images showing sock formation by convection vortex: (a) Before feedstock injection; (b–d) CNT forming closed-end networks, which flow upward around the vortex region; (e) Sock end comes out of the reactor tube; (f) Continuous sock. Experimental conditions: ferrocene concentration is 2 wt%, gas flow rate is 1000 sccm, and feedstock injection rate is 16 ml/h. (A color version of this figure can be viewed online.)

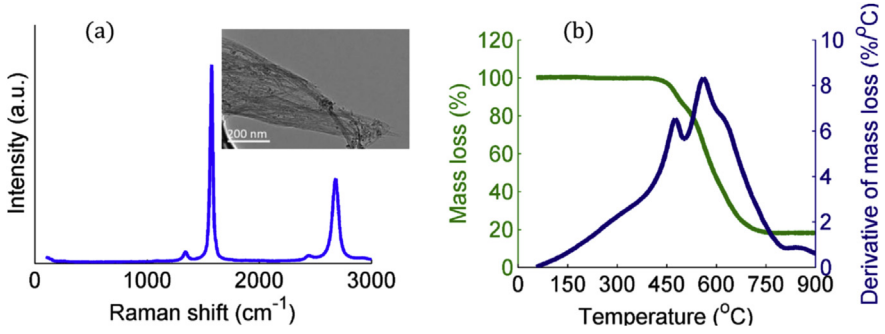

Fig. 6. Properties of the collected CNT sample: (a) Raman microscopy showing G/D ration of 25, insert is sample TEM image; (b) Thermogravimetric analysis of the sample. Experimental conditions: ferrocene concentration is 1 wt%, gas flow rate is 1000 sccm, and feedstock injection rate is 16 ml/h. (A color version of this figure can be viewed online.)

properties of the grown CNTs.

A convection vortex also occurs in vertical furnaces. Simulation of vertical reactor was performed using the same parameters for the simulation of the horizontal furnace. The streamlines are shown in Fig. 7. Previously, Li et al. [1] observed that convection occurred in the upper half of the furnace. They speculated that the gas moved upward close to the furnace walls and downward in the center of the tube, which was confirmed by our simulation (Fig. 7). As the velocity streamline shows, the backflow (Fig. 7 a and b) carries vaporized feedstock upward toward the inlet of the furnace.

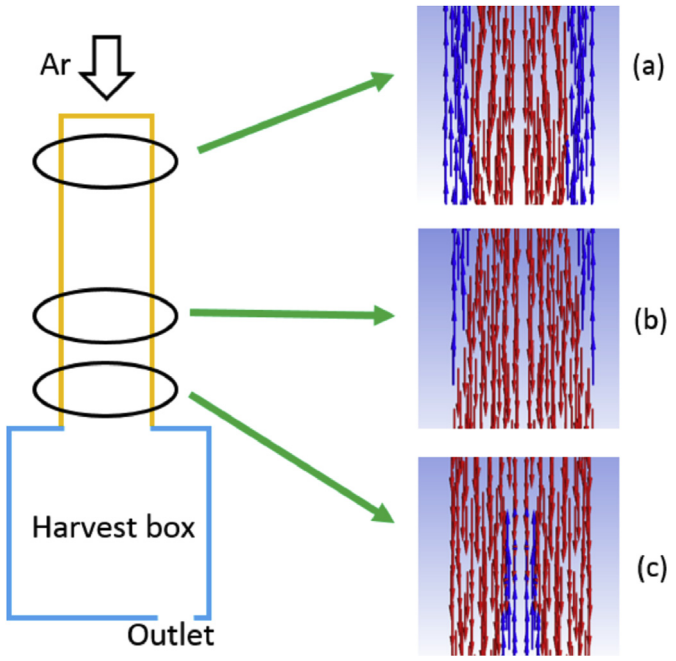

Fig. 7. Streamline in vertical furnace at different parts of the tube: (a) Tube inlet region; (b) Middle region; and (c) Tube outlet region. Red streamlines indicate doward flow and blue streamlines indicate upward backflow. Parameters used are the same as for the horizontal furnace, except the reactor is placed vertically. (A color version of this figure can be viewed online.)

The observed vortex affects the catalyst formation process and later CNT growth. Theoretically the back flow will take some catalyst back towards the inlet. Thus part of the catalyst, hydrocarbon and thiophene will stay for a longer time inside a vertical furnace instead of being carried out quickly. This could explain why there is still sock formation for a certain time after the sulfur is stopped [13]. The reason might be that it takes certain time to purge the remaining sulfur in the reactor, since it is trapped in the inlet vortex.

It was stated that there is no convection in the lower half of the vertical furnace due to density increase [1]. Simulation, however, indicates the convection is significant in the outlet region of the vertical furnace, which might also explain the closed end formation of the sock. Similar as the horizontal furnace, the outlet convection vortex could possibly lead to the formation of the sock closed end, and ensuing continuous sock formation. It should be noted the synthesis processes in horizontal and vertical furnaces are quite different. For example, the flow field is axisymmetric in a vertical furnace and plane symmetric in a horizontal furnace. The two different flow fields might both lead to sock formation due to the convection vortex. This must be further verified by experiment.

3.3. Aerogel-like sock dynamics

Once the sock forms, its behavior can be changed by varying the gas flow rate and feedstock injection rate. Images of socks under various carrier gas flow rates are shown in Fig. 8. The transparency of the sock increases when increasing the gas flowrate, indicating a lower CNT concentration with the higher gas flowrate. For our system, when the carrier gas flowrate is too high of 2000 sccm, there is no sock formation with only random CNTs carried by the flow.

It can be seen that the sock becomes darker with a higher feedstock injection rate (Fig. 8 e–h). The feedstock injection rate determines the initial iron concentration, and thus amount of catalyst available for growth. With other factors remaining the same, a high injection rate increases the overall catalyst concentration, which provides more active catalyst particles capable of nucleating nanotubes. In this horizontal reactor, it was found that the sock diameter increases along with increasing flowrate (Fig. 8 a–c). A similar phenomenon has also been observed in vertical furnace [22]. The speed of the sock exiting the reactor tube increases when increasing the feedstock injection rate. The sock will keep flowing out of the reactor if the end is closed. Typically about a 0.3 m length of the sock extends into a harvest box where the sock is wound up on a motorized pulley.

Although the sock always has a thick shell, the sock inner pattern changes when the feedstock injection or carrier gas flowrate is varied. Sock pattern under 1200 sccm (Fig. 8b) is close to concentric, while 1800 sccm has a more significant vortex (Fig. 8c). With low gas flowrate and slow feedstock injection rate (Fig. 8 e–g), the sock patterns are almost concentric, with a core in the center and a shell surrounding it. Obviously this could not be explained by only using the convection vortex model. It is believed that the patterns changes are due to the interaction between sock and the carrier gas, which is not considered in the previous simulation. By changing the feedstock injection rate and carrier gas flowrate, the concentration of CNTs and the sock permeability will be varied. Also the carrier gas flow could be influenced by the existence of different sock structures. Thus the sock structure and the carrier gas flow will affect each other and ultimately reach stability, leading to various sock patterns.

The sock could be treated as a web-shell structure (Fig. 9), with a shell composed of CNT webs. The sock has a thicker shell and a low-density center. Sometimes the sock center is even transparent. There is vortex inside the sock (Fig. 4), which indicates that the sock should have certain gas permeability to allow convection happen. The near hollow sock could sustain a certain pressure and driving force because of the thick shell (~100 nm thick wall) and closed end. The thickness of the shell should affect the gas permeability as well as the driving force acting on the sock. The gas permeability of the sock and the carrier gas flow rate, control the sock formation and its speed exiting the reactor. For successful sock formation, the shell thickness should be high enough to maintain the structural shape under the carrier gas flow. For too high gas flowrate (Fig. 8d), the web-shell structure could not be sustained resulting failure of sock formation.

Cranford et al. [33] modeled the effect of wind on a spider web. Similarly, the drag force on a CNT sock could be expressed as:

$$F_d = \frac{1}{2} N \rho_{gas} u^2 C_D A \tag{4}$$

Here N is the number of CNTs under load, ρ_{gas} is the gas density, u the mean gas flow speed, A the reference area of the fiber ($A = dl$ fiber diameter multiplied by fiber length), and C_D the drag coefficient in the flow direction.

This partly explains the increase of sock speed with higher feedstock injection rate. The higher feedstock injection rate leads to a larger concentration of catalyst particles, resulting an increase of the number of CNTs. Based on equation (4), the driving force on the sock will increase due to more CNTs under load. As for the change of the sock diameter under different flowrates (Fig. 7), it could be related to the force acting on the sock. With a higher flowrate, the force on the sock increases, which is responsible for both pushing the sock out of the reactor tube, and expanding it radially. Thus a higher flowrate leads to a larger sock whose diameter is close to the tube diameter. There exists a critical length of the furnace to achieve continuous growth and to obtain long CNT and provide the

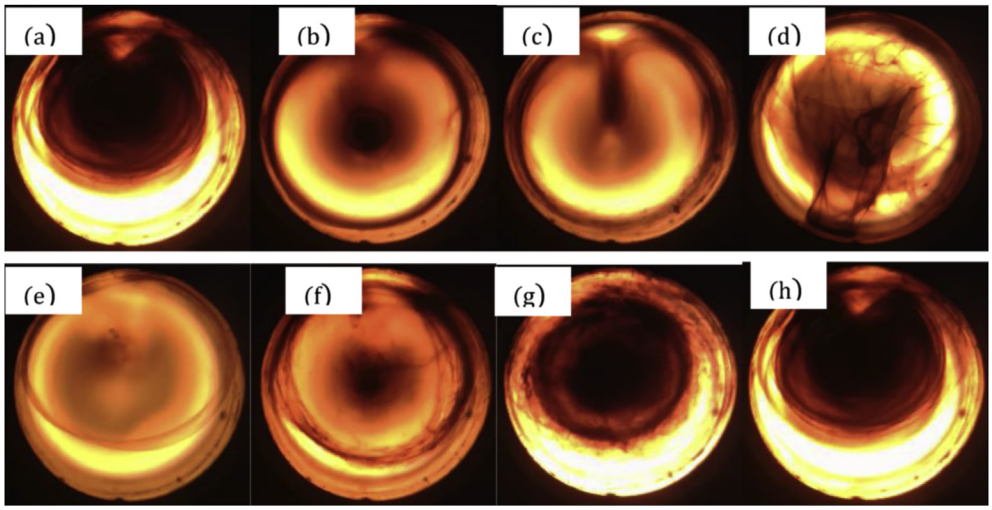

Fig. 8. Morphology of sock formation under different gas flow rates and feedstock injection rates: (a) 800 sccm; (b) 1200 sccm; (c) 1800 sccm thinner sock; and (d) 2000 sccm no sock. In (a–d) the feedstock injection rate is 32 ml/h, ferrocene 1 wt%. In (e–h) gas flowrate 800 sccm, ferrocene 1 wt%, and feedstock injection rate of (e) 8 ml/h and (f) 16 ml/h (g) 24 ml/h (h) 32 ml/h. (A color version of this figure can be viewed online.)

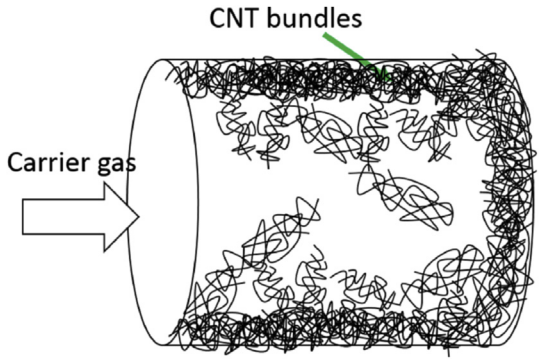

Fig. 9. Schematic of the web-shell structure. (A color version of this figure can be viewed online.)

best properties for the thread or sheet. The influence of furnace length on the CNT web-shell structure will be investigated in the future.

It is clear that the previous simulation and analysis did not consider the feedstock evaporation and influence of the sock on the flow field, which are both important to the process. A better model and simulation, accounting for feedstock evaporation and the two-way interaction between the gas flow and sock, is currently being developed to provide a deeper understanding of the synthesis of CNTs by floating catalyst method. And it could possibly be used as a tool to optimize the reaction parameters to form a sock that provides the highest properties for the yarn and sheet produced.

4. Conclusions

Aerogel-like sock formation has been investigated in this study. A more complete sock formation mechanism based on a convection vortex mechanism has been proposed, stemming from experimental evidence and verified by simulation. The sock dynamic behavior was observed under varied conditions of feedstock injection rate and carrier gas flow rates. A web-shell structure was used to explain the sock formation behavior. The influence of the various sock conditions on the properties of CNT yarn/sheet is currently under further study. The knowledge gained in this work will guide future optimization of the CNT sock formation process and contribute to better control over the properties of CNT products fabricated from yarn and sheet.

Acknowledgments

This work was supported by NSF Award 1120382 under Program Managers Dr. Bruce Kramer and Dr. Khershed P. Cooper, the University of Cincinnati, College of Engineering under Associate Dean for Research Dr. Tim Keener, and ONR Award N00014-15-1-2473 under Program Manager Dr. Ignacio Perez.

References

[1] Y.-L. Li, I.A. Kinloch, A.H. Windle, Direct spinning of carbon nanotube fibers from chemical vapor deposition synthesis, Science 304 (5668) (2004) 276–278.
[2] M. Motta, Y.L. Li, Kinloch Ia, aH. Windle, Spun fibers of carbon nanotubes, Nano Lett. 5 (8) (2005) 1529–1533.
[3] W. Ren, F. Li, S. Bai, H.-M. Cheng, The Effect of sulfur on the structure of carbon nanotubes produced by a floating catalyst method, J. Nanosci. Nanotechnol. 6 (5) (2006) 1339–1345.
[4] B. Alemán, V. Reguero, B. Mas, J.J. Vilatela, Strong carbon nanotube fibers by drawing inspiration from polymer fiber spinning, ACS Nano 9 (7) (2015) 7392–7398.
[5] J.N. Wang, X.G. Luo, T. Wu, Y. Chen, High-strength carbon nanotube fibre-like ribbon with high ductility and high electrical conductivity, Nat. Commun. 5 (2014), 3848-.
[6] K. Koziol, J. Vilatela, A. Moisala, M. Motta, P. Cunniff, M. Sennett, et al., High-performance carbon nanotube fiber, Sci. (New York, NY) 318 (5858) (2007) 1892–1895.
[7] X.H. Zhong, Y.L. Li, Y.K. Liu, X.H. Qiao, Y. Feng, J. Liang, et al., Continuous multilayered carbon nanotube yarns, Adv. Mater. 22 (2010) 692–696.
[8] M.W. Schauer, D. Lashmore, B. White, Synthesis and properties of carbon nanotube yarns and textiles, MRS Proc. 1081 (2008), 1081–P03–P05.
[9] V. Reguero, B. Alemán, B. Mas, J.J. Vilatela, Controlling carbon nanotube type in macroscopic fibers synthesized by the direct spinning process, Chem. Mater. 26 (11) (2014) 3550–3557.
[10] C. Paukner, K.K.K. Koziol, Ultra-pure single wall carbon nanotube fibres continuously spun without promoter, Sci. Rep. 4 (2014), 3903-.
[11] M. Motta, A. Moisala, Kinloch Ia, A.H. Windle, High Performance Fibres from 'Dog Bone' Carbon Nanotubes, Adv. Mater. 19 (21) (2007) 3721–3726.
[12] K.-H. Lee, S.-H. Lee, J. Park, H.-R. Kim, J. Lee, Synthesis of high-quality carbon nanotube fibers by controlling the effects of sulfur on the catalyst agglomeration during the direct spinning process, RSC Adv. (2015) 41894–41900.
[13] T.S. Gspann, F.R. Smail, A.H. Windle, Spinning of carbon nanotube fibres using the floating catalyst high temperature route: purity issues and the critical role of sulphur, Faraday Discuss. 173 (0) (2014) 47–65.
[14] Y.-L. Li, L.-H. Zhang, X.-H. Zhong, A.H. Windle, Synthesis of high purity single-walled carbon nanotubes from ethanol by catalytic gas flow CVD reactions,

Nanotechnology 18 (2007), 225604-.
[15] Y.-L. Li, Kinloch Ia, A.H. Windle, Direct spinning of carbon nanotube fibers from chemical vapor deposition synthesis, Sci. (New York, NY) 304 (5668) (2004) 276–278.
[16] M. Motta, I. Kinloch, A. Moisala, V. Premnath, M. Pick, A. Windle, The parameter space for the direct spinning of fibres and films of carbon nanotubes, Phys. E Low-dimens. Syst. Nanostruct. 37 (1–2) (2007) 40–43.
[17] Z. Li, Z. Liu, H. Sun, C. Gao, Superstructured assembly of nanocarbons: fullerenes, nanotubes, and graphene, Chem. Rev. 115 (15) (2015) 7046–7117.
[18] J.J. Vilatela, A.H. Windle, Yarn-like carbon nanotube fibers, Adv. Mater. 22 (d) (2010) 4959–4963.
[19] J. Benson, I. Kovalenko, S. Boukhalfa, D. Lashmore, M. Sanghadasa, G. Yushin, Multifunctional CNT-polymer composites for ultra-tough structural supercapacitors and desalination devices, Adv. Mater. 25 (Cdi) (2013) 6625–6632.
[20] A.S. Wu, X. Nie, M.C. Hudspeth, W.W. Chen, T.W. Chou, D.S. Lashmore, et al., Strain rate-dependent tensile properties and dynamic electromechanical response of carbon nanotube fibers, Carbon 50 (10) (2012) 3876–3881.
[21] Z.P. Wu, X.L. Huang, B. Li, Y.H. Yin, Y.S. Li, Y.S. Chen, et al., Strong carbon nanotube macro-films with retained deformability at fairly low temperatures, Phys. E Low-dimens. Syst. Nanostruct. 47 (2013) 285–289.
[22] D. Conroy, A. Moisala, S. Cardoso, A. Windle, J. Davidson, Carbon nanotube reactor: ferrocene decomposition, iron particle growth, nanotube aggregation and scale-up, Chem. Eng. Sci. 65 (10) (2010) 2965–2977.
[23] D.P. Brown, A.G. Nasibulin, E.I. Kauppinen, CFD-aerosol modeling of the effects of wall composition and inlet conditions on carbon nanotube catalyst particle activity, J. Nanosci. Nanotechnol. 8 (8) (2008) 3803–3819.
[24] K. Kuwana, K. Saito, Modeling CVD synthesis of carbon nanotubes: nanoparticle formation from ferrocene, Carbon 43 (10) (2005) 2088–2095.
[25] H. Endo, K. Kuwana, K. Saito, D. Qian, R. Andrews, Grulke Ea, CFD prediction of carbon nanotube production rate in a CVD reactor, Chem. Phys. Lett. 387 (2004) 307–311.
[26] L. Samandari-masouleh, N. Mostou, A. Khodadadi, Y. Mortazavi, M. Maghrebi, Modeling the Growth of Carbon Nanotubes in a Floating Catalyst Reactor, 2012, pp. 1143–1149.
[27] K. Kuwana, R. Andrews, Grulke Ea, K. Saito, CFD analysis on a vortex enhanced CVD reactor design, MRS Proc. 706 (2001). Z3.12.1–Z3.1.
[28] X.-H. Zhong, Y.-L. Li, J.-M. Feng, Y.-R. Kang, S.-S. Han, Fabrication of a multifunctional carbon nanotube “cotton” yarn by the direct chemical vapor deposition spinning process, Nanoscale 4 (2012), 5614-.
[29] J. Chaffee, D. Lashmore, D. Lewis, J. Mann, M. Schauer, B. White, Direct synthesis of CNT yarns and sheets, in: Nsti Nanotech 2008, Vol 3, Technical Proceedings, 3, 2008, pp. 118–121.
[30] J. Blazek, Chapter 2-governing equations, in: J. Blazek (Ed.), Computational Fluid Dynamics: Principles and Applications, third ed., Butterworth-Heinemann, Oxford, 2015, pp. 7–27.
[31] Raji K, Sobhan C. A computational model for predicting the mass transport in a CVD reactor for carbon nanotube synthesis. Fourth International Conference on Smart Materials and Nanotechnology in Engineering: International Society for Optics and Photonics; p. 87931N-N-9.
[32] A. Fluent, Theory Guide and User's Guide, Ansys Inc, USA, 2015.
[33] S.W. Cranford, A. Tarakanova, N.M. Pugno, M.J. Buehler, Nonlinear material behaviour of spider silk yields robust webs, Nature 482 (7383) (2012) 72–76.